A finite element analysis of impact damage in composite laminates

Y. Shi
mep10ys@sheffield.ac.uk
Department of Mechanical Engineering (Aerospace)
University of Sheffield
Sheffield, UK

C. Soutis
constantinos.soutis@manchester.ac.uk
School of Mechanical, Aerospace & Civil Engineering
University of Mancheste
Manchester, UK

ABSTRACT

In this work, stress-based and fracture mechanics criteria were developed to predict initiation and evolution, respectively, of intra- and inter-laminar cracking developed in composite laminates subjected to low velocity impact. The Soutis shear stress-strain semi-empirical model was used to describe the nonlinear shear behaviour of the composite. The damage model was implemented in the finite element (FE) code (Abaqus/Explicit) by a user-defined material subroutine (VUMAT). Delamination (or inter-laminar cracking) was modelled using interface cohesive elements and the splitting and transverse matrix cracks that appeared within individual plies were also simulated by inserting cohesive elements between neighbouring elements parallel to the fibre direction in each single layer. A good agreement was obtained when compared the numerically predicted results to experimentally obtained curves of impact force and absorbed energy versus time. A non-destructive technique (NDT), penetrant enhanced X-ray radiography, was used to observe the various damage mechanisms induced by impact. It has been shown that the proposed damage model can successfully capture the internal damage pattern and the extent to which it was developed in these carbon fibre/epoxy composite laminates.

Paper No. 3860. Manuscript received 27 June 2012, revised version received 13 September 2012, accepted 27 September 2012.

NOMENCLATURE

d^t	Tensile damage variable
d^c	Compressive damage variable
G^T	Tensile fracture toughness, kJ/m^2
G^C	Compressive fracture toughness, kJ/m^2
G^0	Shear modulus, GPa
K	Interface normalized stiffness, GPa/mm
l^*	Characteristic length, mm
N, S, T	Interlaminar normal and shear strengths, MPa
S^{12}	In-plane shear strength, MPa
S^{23}	Out-of-plane shear strength, MPa
S^A_{23}	Transverse shear strength in fracture plane, MPa
$\mathbf{T}(\alpha)$	Transformation matrix
X^T	Fibre tensile strength, MPa
X^C	Fibre compressive strength, MPa
Y^T	Matrix tensile strength, MPa
α	Orientation of the fracture plane
β	Mode mixity ratio
δ	Displacement
ε^0	Strain for damage initiation
ε^f	Strain for completed damage
η	Power law
σ	Stress tensor, MPa
κ	Shear factor
τ	Shear stress, Mpa
γ	Shear strain
μ	Friction coefficient

1.0 INTRODUCTION

Polymer composite structures mainly consist of a resin system (thermoset or thermoplastic matrix) reinforced by continuous fibres (carbon, glass or aramid) and exhibit a relatively brittle behaviour and complicated damage patterns that develop internally and are thus difficult to detect[1,2]. When a composite laminate is subjected to static or fatigue loading, internal damage occurs in the form of resin cracking and delamination that leads to loss of stiffness and eventually load-carrying capability when fibres break. Thus, it is important to understand and model the progressive damage of composite laminates in the design and fabrication of aircraft structural components[3].

In general, damage to composite structures may result in two main failure modes: (*i*) Intralaminar failure that occurs within a ply and can be expressed by modes such as tensile and compressive fibre breakage[4,5], tensile and compressive matrix damage[6] and damage between the fibre and matrix interface (splitting or debonding). Matrix cracking and fibre/matrix splitting have been recognised as resin dominated damage modes and have been studied extensively. (*ii*) Interlaminar failure (delamination) that occurs between neighbouring plies, which is initiated by intralaminar damage such as transverse ply cracking[7-12].

Damage mechanisms for a thin plate subjected to impact loading can be categorized as low and high velocity scenarios; perforation is more likely to occur during a high velocity impact of a thin

https://doi.org/10.1017/S0001924000007661 Published online by Cambridge University Press

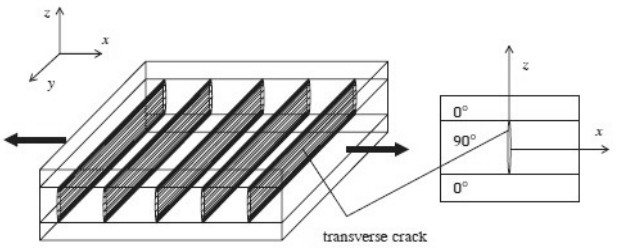

Figure 1. A schematic of a cross-ply laminate with transverse matrix cracks[21].

plate, while for a low velocity impact there is a sufficiently long contact duration to introduce internal matrix cracking, delamination and fibre breakage that spreads over a larger area[13]. The finite element (FE) technique has been considered for development of a numerical model that could accurately describe the impact and predict the complex internal damage mechanisms in a relatively short time. This approach is desirable for avoiding the considerably expensive and time consuming process of performing the experiment. Constitutive models provided by several analytical studies may form that basis for simulation of the complicated composite material behaviour[13-17]. Recent research, based on continuum damage mechanics (CDM), on modelling the damage of composite laminates subjected to impact has been reported[15-18]. This was initiated by the work of Kachanov[19] and Rabotnov[20]. In addition, Soutis *et al*[7,8] further developed the equivalent constraint model (ECM)[9] of a damaged lamina to successfully predict the effect of matrix cracking and matrix crack induced delamination on stiffness degradation.

In this paper, the impact induced damage was modelled by implementing a user-defined 3D damage model (VUMAT) with solid elements into the finite element code Abaqus/Explicit. Interface cohesive elements were inserted between neighbouring plies to simulate delamination, and also used to model the splitting and transverse matrix cracks by inserting them between adjacent elements along the fibre direction with the assumption of equally spaced cracks as illustrated in Fig. 1[21].

An effective approach developed by Soutis *et al*[4,5] and validated by experiment has also been used to describe the nonlinear shear behaviour of the laminate that affects the depth of indentation during the impact event. A general contact algorithm was defined with appropriate contact pair properties to simulate the contact between impactor and composite plate surface, and the contact between layers. The numerical results from the simulation were evaluated by comparing with experimental measurements and observations and this demonstrated the ability of the proposed damage modelling approach to predict the type and extent of impact induced damage.

2.0 COMPOSITE DAMAGE MODEL FOR IMPACT

2.1 Damage initiation and evolution

Damage modelling in composites can be studied either by stress or strain-based failure criteria approach or following damage mechanics concepts. The polynomial failure criteria, such as the Tsai-Wu or Tsai-Hill, based on the equivalent stress or strain are usually employed to describe the

https://doi.org/10.1017/S0001924000007661 Published online by Cambridge University Press

failure envelope of any given multidirectional laminate subjected to multi-axial loading. However, the damage mechanisms as different modes cannot be clearly characterised using the polynomial failure criteria.

Hashin proposed a failure criterion for a unidirectional composite as a ply-by-ply method to separately model four distinct failure modes: failure of fibres in tension and compression and matrix tensile and compressive failure[22,23]. Hashin failure criterion has been used extensively in industry, although it cannot accurately predict the matrix compressive failure initiation. Thus, in the present study, the Hashin criterion is used to estimate the fibre and tensile matrix damage initiation, while the damage model developed by Puck and Schurmann[24] is used to model matrix compressive failure, i.e.

Fibre tensile failure ($\hat{\sigma}_{11} \geq 0$):

$$F_{ft} = \left(\frac{\hat{\sigma}_{11}}{X^T}\right)^2 + \kappa\left(\frac{\hat{\sigma}_{12}}{X_T}\right)^2 = 1 \quad \ldots (1)$$

Fibre compressive failure ($\hat{\sigma}_{11} < 0$):

$$F_{fc} = \left(\frac{\hat{\sigma}_{11}}{X^C}\right)^2 = 1 \quad \ldots (2)$$

Matrix tensile failure ($\hat{\sigma}_{22} \geq 0$):

$$F_{mt} = \left(\frac{\hat{\sigma}_{22}}{Y^T}\right)^2 + \left(\frac{\hat{\sigma}_{12}}{S_{12}}\right)^2 + \left(\frac{\hat{\sigma}_{23}}{S_{23}}\right)^2 = 1 \quad \ldots (3)$$

Matrix compressive failure ($\hat{\sigma}_{22} < 0$):

$$F_{mc} = \left(\frac{\sigma_{TN}}{S_{23}^A + \mu_{TN}\sigma_{NN}}\right)^2 + \left(\frac{\sigma_{LN}}{S_{12} + \mu_{LN}\sigma_{NN}}\right)^2 = 1 \quad \ldots (4)$$

In Equations (1-4), $\hat{\sigma}_{ij}(i,j = 1, 2, 3)$ is the effective stress tensor, X^T and X^C denote the tensile and compressive strengths of the unidirectional composite laminate in the fibre direction, Y^T is the tensile in the transverse direction, $S_{i,j}$ $(i,j = 1, 2, 3)$ denotes the longitudinal and transverse shear strengths of the composite, respectively. The coefficient κ in Equation (1) accounts for the contribution of shear stress on fibre tensile failure, which is ignored in the present study. In Equation (4) σ_{ij} $(i,j = L, T, N)$ is the stress tensor σ_{ij} $(i,j = 1, 2, 3)$ rotated to the fracture plane by using the transformation matrix $T(\alpha)$:

$$\sigma_{LTN} = T(\alpha)\sigma_{123}T(\alpha)^T \quad \ldots (5)$$

S_{23}^A is the transverse shear strength in the fracture plane, which can be determined by the transverse compression strength and the angle of fracture plane. The key concept of Puck's failure criterion is to determine the inclination or orientation of the fracture plane by calculating the angle, α, as shown in Fig. 2.

In order to predict damage development in the laminate, a stiffness degradation rule needs to be defined. The damage evolution procedure is based on a strain failure criterion where the strain

https://doi.org/10.1017/S0001924000007661 Published online by Cambridge University Press

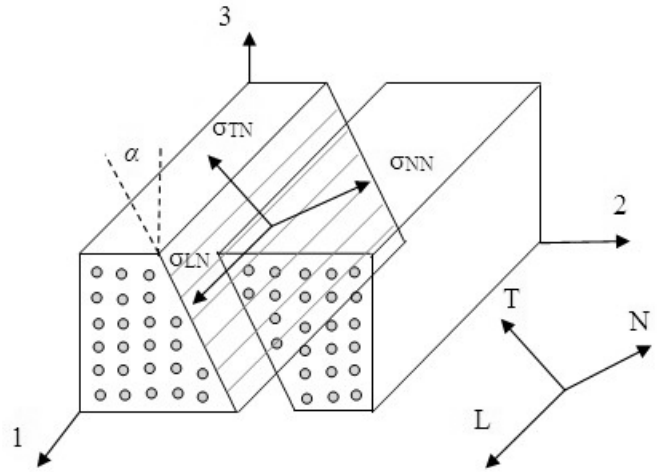

Figure 2. Fracture plane for matrix compressive failure relative to material co-ordinate system.

tensor is continuously updated with increasing load for each material point associated with each different failure mechanism.

According to previous work[15-17], the stresses in the fibre direction are predominantly carried by the fibres because of their high stiffness and strength. When the damage initiation criterion is met, Equations (1) and (3), the material properties are gradually degraded, by using the following damage variable where for fibre and matrix tensile failure is expressed as:

$$d_{1,2}^{T} = \frac{\varepsilon_{1,2}^{fT}}{\varepsilon_{1,2}^{fT} - \varepsilon_{1,2}^{0T}}\left(1 - \frac{\varepsilon_{1,2}^{0T}}{\varepsilon_{1,2}}\right) \quad \ldots (6)$$

where the subscript 1 and 2 denote the fibre and transverse direction, respectively; $\varepsilon_{1,2}^{0T}$ is the tensile strain for damage initiation. Due to the irreversibility of the damage variable, the strain calculated at each time step is defined as $\varepsilon_{1,2} = max(\varepsilon_{1,2}, \varepsilon_{1,2}^{0T})$ in Equation (6). In order to avoid zero or negative energy absorption due to damage, the final failure strain needs to be greater than the initial failure strain, i.e. $\varepsilon_{1,2}^{fT} > \varepsilon_{1,2}^{0T}$. $\varepsilon_{1,2}^{fT}$ denotes the tensile strain at final failure at which the damage variable is equal to one. The $\varepsilon_{1,2}^{fT}$ is derived from the fracture toughness $G_{1,2C}^{T}$ associated with fibre (1) or matrix (2) tensile failure, the failure strength of the material (X^T or Y^T) and the characteristic length l^*:

$$\varepsilon_{1}^{fT} = \frac{2G_{1C}^{T}}{X^{T} l^{*}} \quad \ldots (7a)$$

$$\varepsilon_{2}^{fT} = \frac{2G_{2C}^{T}}{Y^{T} l^{*}} \quad \ldots (7b)$$

where l^* is the characteristic length that would keep a constant energy release rate per unit area of crack and make the final results independent of *FE* mesh size. In this work the approach developed by Bažant and Oh[25] was used which has been shown to be computationally efficient and to work reasonably well for solid elements[26] and for a solid element l^* is given by

$$l^{*} = \frac{\sqrt{A_{IP}}}{\mathrm{Cos}\theta} \quad |\theta| \leq 45^{\circ} \quad \ldots (8)$$

https://doi.org/10.1017/S0001924000007661 Published online by Cambridge University Press

Similarly, the compressive damage variable can be expressed in the same way. However, it is noticed that for matrix compressive failure, the damage evolution should be effectively predicted under the fracture plane defined rather than the plane in global coordinate.

2.2 Delamination using interface cohesive elements

In the work by Camanho and Dávila[27] a stress based failure criterion to predict damage initiation was employed, while delamination propagation was based on fracture mechanics concepts where an interface element was introduced between each ply of the composite laminate. The stress failure criterion used to estimate the delamination onset is given by:

$$\left(\frac{\sigma_n}{N}\right)^2+\left(\frac{\sigma_s}{S}\right)^2+\left(\frac{\sigma_t}{T}\right)^2=1 \qquad \ldots (9)$$

where σ_i ($i = n, s, t$) denotes the traction stress vector in the normal n and shear directions, s and t, respectively, while N, S and T are defined as the corresponding inter-laminar normal and two shear strengths.

The traction stress σ_i can be calculated as given in the Abaqus manual[28] using the stiffness in Modes I, II and III and the opening and/or sliding displacements δ_i:

$$\sigma_i = K_i, \delta_i,\ i = n,s,t \qquad \ldots (10)$$

Once the damage initiation criterion has been reached, the material stiffness is gradually degraded in terms of a damage variable d. Its values range from zero when damage initiates to one ($d = 1$) when complete delamin`ation has occurred in the interface element. The failure criterion to predict delamination propagation under mixed-mode loading is expressed in terms of the energy release rates associated with Modes I, II and III. For a linear softening process the damage variable d for delamination evolution is defined as:

$$d=\frac{\delta_m^f\left(\delta_m^{max}-\delta_m^0\right)}{\delta_m^{max}\left(\delta_m^f-\delta_m^0\right)} \qquad \ldots (11)$$

where δ_m^{max} refers to the maximum value of the mixed-mode displacement attained during the loading history. The δ_m parameter corresponds to the total mixed-mode displacement (normal, sliding, tearing) given by:

$$\delta_m=\sqrt{\delta_n^2+\delta_s^2+\delta_t^2} \qquad \ldots (12)$$

In Equation (11) δ_m^f is the mixed-mode displacement at complete failure and δ_m^0 is the effective displacement at damage initiation. A Benzeggagh–Kenane (BK) fracture energy based criterion[27] can be used to define the mixed-mode displacement for complete failure, δ_m^f:

$$\delta_m^f=\begin{cases}\frac{2}{K\delta_m^0}\left[G_{IC}+\left(G_{IIC}-G_{IC}\right)\xi^{\eta}\right] & \delta>0\\ \sqrt{\left(\delta_s^f\right)^2+\left(\delta_t^f\right)^2} & \delta_n\le 0\end{cases} \qquad \ldots (13)$$

where η is the B-K power law parameter that can be determined using a least-square fit from a

https://doi.org/10.1017/S0001924000007661 Published online by Cambridge University Press

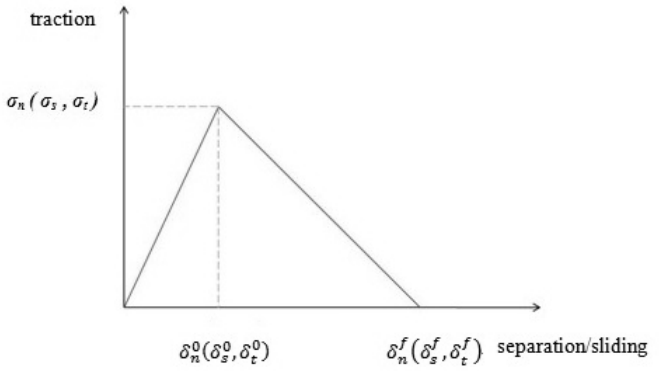

Figure 3. Typical traction-displacement relationship.

set of mixed-mode bending experimental data; $\left(\xi = \frac{\beta^2}{1+\beta^2}\right)$ with ξ taking values between zero and one. When $\xi = 0$ fracture is mode I driven, while as $\xi \rightarrow 1$ is Mode II dominated (and this is also the case when $\eta = 0$). β is the mode mixity ratio $\left(= \frac{\delta_s}{\delta_n}\right)$.

A typical linear traction-separation model used for fracture Modes I, II and III is shown in Fig. 3. Initially, the linear elastic response is represented using the stiffness K_i ($i = n, s, t$). Once the normal or shear tractions reach the corresponding inter-laminar normal and shear strengths, delamination will be initiated and then the stiffness will start to degrade linearly according to the damage evolution variable d given by Equation (11).

2.3 Nonlinear shear behaviour

In general composite laminates always show a nonlinear and irreversible shear behaviour according to the experimental observations. There are several approaches to model the nonlinear shear behaviour of the composite laminate published in the literature such as continuum theories of plasticity[29], continuum damage mechanics[30], or combination of these two methods[31]. In this paper, a semi-empirical expression developed by Soutis *et al*[4,5] is used to represent the nonlinear shear response.. The nonlinear shear stress-strain relations are expressed by Equation (14):

$$\tau_{i,j} = S_{i,j}\left[1 - \exp\left(-\frac{G_{i,j}^0 \gamma}{S_{i,j}}\right)\right], \quad i,j = 1,2,3 \qquad \ldots (14)$$

The ultimate shear strength $S_{i,j}$ and the elastic shear modulus $G_{i,j}^0$, both of which are composite materials constants and readily measurable, are required for implementation in the *FE* program that models the nonlinear shear behaviour of the composite.

The nonlinear shear damage is successfully simulated using a strain-based damage initiation and evolution criterion as shown Fig. 4. The strain in this nonlinear shear model is decomposed into

https://doi.org/10.1017/S0001924000007661 Published online by Cambridge University Press

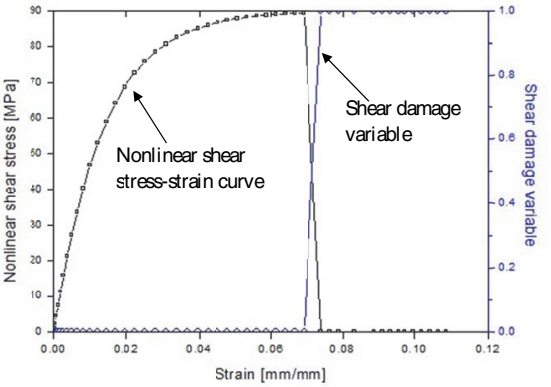

Figure 4. Nonlinear shear behaviour using the Soutis model with shear damage variable.

two parts: elastic strain $\gamma_{i,j}^{e}$ and plastic strain $\gamma_{i,j}^{in}$. The inelastic strain is defined as:

$$\gamma_{i,j}^{in} = \gamma_{i,j} - \gamma_{i,j}^{e} = \gamma_{i,j} - \frac{\tau_{i,j}}{G_{i,j}^{0}} \quad \ldots (15)$$

where $\tau_{i,j}$ is the nonlinear shear stress corresponding to the different shear planes; $G_{i,j}^{0}$ is the original shear modulus. Similarly, the criterion of initiation of shear failure is expressed in terms of the nonlinear shear stress and maximum shear strength:

$$F_{i,j}^{S} = \frac{\left|\tau_{i,j}\right|}{S_{i,j}} = 1, \qquad i,j = 1,2,3 \quad \ldots (16)$$

where $\tau_{i,j}$ is the shear stress at the given shear plane and $S_{i,j}$ indicates the relative ultimate shear strength in that plane. The damage evolution law for the nonlinear shear modes is expressed by the damage variable $d_{i,j}$:

$$d_{i,j} = \frac{\gamma_{i,j}^{rf}\left[2\left(\gamma_{i,j} - \gamma_{i,j,0}^{in}\right) - \gamma_{i,j}^{f}\right]}{\left(\gamma_{i,j}^{f} + \gamma_{i,j,0}^{in} - \gamma_{i,j}\right)\left(\gamma_{i,j} - \gamma_{i,j,0}^{in}\right)} \quad \ldots (17)$$

3.0 EXPERIMENT AND SIMULATION FOR IMPACT

3.1 Impact test

Composite laminate plates with a thickness of 2mm were fabricated from carbon fibre/epoxy resin prepreg with a stacking sequence of $[0/90]_{2s}$. The prepreg was made from continuous unidirectional high tensile strength carbon fibres (Tenax HTS40 12K 300) impregnated with Cycom® 977-2 epoxy resin, which is a typical high temperature curing aerospace grade system. The laminates were autoclave cured following the manufacturer's recommended schedule and cut into specimens measuring 100mm × 100mm.

https://doi.org/10.1017/S0001924000007661 Published online by Cambridge University Press

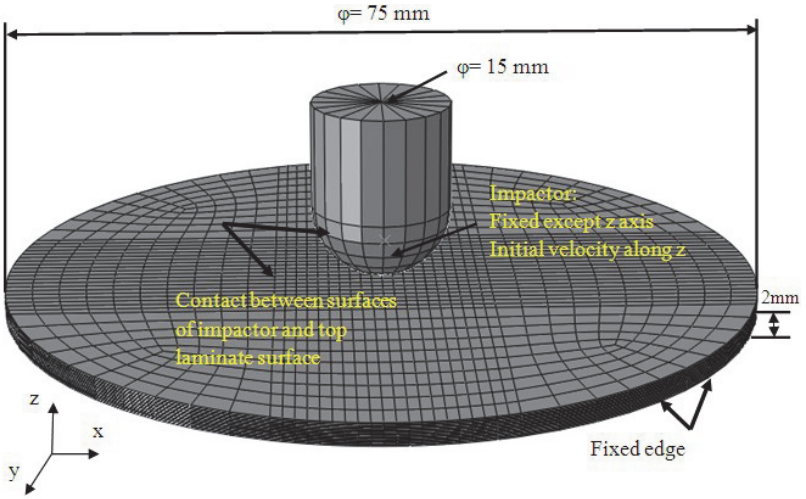

Figure 5. FE model used for the numerical simulation of the impact event.

The impact test was performed following the guidelines ASTM D7136/D7136M-07 standard[32]. The impactor had a hemispherical head of 15mm in diameter, and the tested panels were clamped between two steel plates with a circular exposed area of 75mm in diameter. A consistent impact height 0·75m was used and the mass of the impactor was equal to 1, 1·5 and 2kg resulting in impact energies of 7·35, 11·03 and 14·7J, respectively. Force data were logged from the impactor using a high speed data acquisition unit. For each impact energy case there are at least three panels were tested.

3.2 Simulation of impact

The impact event was simulated by the commercial code Abaqus/Explicit with the proposed failure initiation and fracture criteria together defined by user subroutine VUMAT. Appropriate geometrical models were built and kinematic and loading boundary conditions were defined to represent the experimental set up.

3.2.1 Numerical model

A 3D FE model was built with detailed specifications and boundary conditions shown in Fig. 5. The composite plate was made by the eight-node linear brick element as the unsupported circular shape of 75mm in diameter followed the clamp design. At each ply interface, cohesive elements were inserted with a thickness of 0·0075 mm and were used to model delamination initiation and growth. The 2mm thick laminate consisted of eight plies with a ply thickness of 0·25mm in the stacking sequence $[0/90]_{2s}$. Global and local coordinates were defined to account for ply orientations and correctly describe the laminate and material behaviour. The impactor was modelled as a rigid body; the impact events were performed for the three energies mentioned earlier and a prescribed initial velocity of 3·83 ms^{-1} was assigned to the impactor. Due to the large number of elements used (34,500 in total of solid and extremely thin cohesive elements) in this numerical model, the computation time was approximately 50 hours.

https://doi.org/10.1017/S0001924000007661 Published online by Cambridge University Press

Table 1
Material properties of the carbon fibre/epoxy unidirectional laminate[16,33]

Density (kg/m^3)	**1,600**
Orthotropic properties	E_1^0=153GPa; $E_2^0 = E_3^0$ =10·3GPa; $\nu_{12} = \nu_{13} = 0{\cdot}3$; $\nu_{23} = 0{\cdot}4$; $G_{12}^0 = G_{13}^0 = 6$GPa; $G_{23}^0 = 3{\cdot}7$GPa
Strength (MPa)	$X^T = 2{,}537$; $X^C = 1{,}580$; $Y^T = 82$; $Y^C = 236$; $S_{12} = 90$; $S_{23} = 40$
In-plane fracture toughness (kJ/m^2)	$G_{1C}^T = 91{\cdot}6$; G_{1C}^C=79·9; $G_{2C}^T = 0{\cdot}22$; $G_{2C}^C = 1{\cdot}1$; $G_S = 0{\cdot}7$

Table 2
Material parameters used in the interface cohesive elements[34,35]

	Mode I	Mode II	Mode III
Normalised elastic modulus (GPa/mm)	1,373·3	493·3	493·3
Inrerlaminar strength (MPa)	62·3	92·3	92·3
Interlaminar fracture toughness (kJ/m^2)	0·28	0·79	0·79

3.2.2 Material properties

Table 1 gave the material properties of single lamina[16,33]. The values of fracture toughness for intra- and inter-laminar damage modes were taken from the Refs 34 and 35. The properties of the cohesive elements layers were defined in Table 2 including the values of the elastic modulus, strength and fracture energy, respectively; the stiffness properties were normalised by the element thickness. Damage evolution was taken into account as mixed-mode and the factor defined by Benzeggagh–Kenane fracture energy law[27] was η=1·45, which was experimentally obtained.

3.2.3 Contact algorithm

The general contact algorithm within Abaqus/Explicit was employed to define contact between the impactor and impacted plate and between each neighboured plies of the laminate, respectively. The contact forces based on the penalty enforcement contact method was generated and as a key factor of contact pair properties the friction coefficient in this method was defined as a function of fibre orientation[36-38]. So for a 0°/0° interface the value of μ = 0·2 was reported, while a value of 0·8 was suggested for the interface between neighbouring 90° plies. Thus, in the present analysis an average friction coefficient of 0·5 was used between the 0°/90° interface of the cross ply laminate. In addition, a similar contact algorithm was applied between the surface of the metal impactor and the composite plate and a friction coefficient value of μ= 0·3 was used. It needs to be said that these assumed μ values do have an effect on force time history and hence energy absorbed prediction, so ideally should be measured for the system examined, something that is planned for future work.

https://doi.org/10.1017/S0001924000007661 Published online by Cambridge University Press

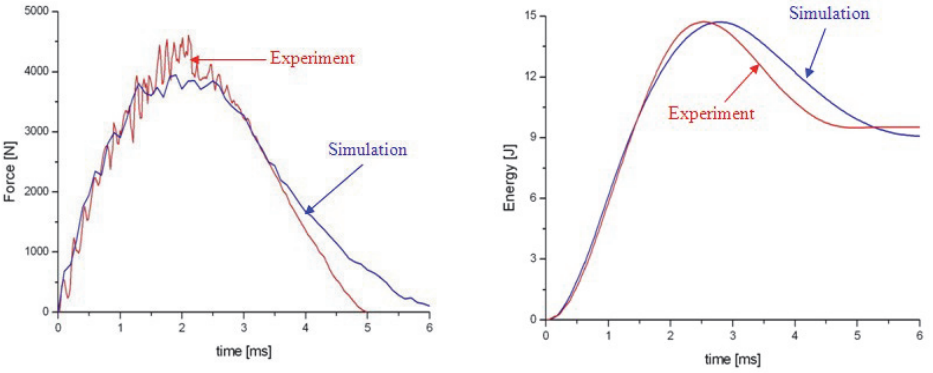

(a) (b)

Figure 6. Experimental and numerical impact results at an impact energy level of 14·7J
(a) Force-time history and (b) Energy-time history.

4.0 RESULTS AND DISCUSSION

4.1 Impact force & energy

A typical experimentally and numerically obtained force-time history curve for impact energy of 14·7J is shown in Fig. 6(a). Initially some oscillations can be seen due to the elastic vibration induced by the initial contact between the impactor and the composite laminate. After that, intense oscillations start to occur near the peak force value that indicates that damage has occurred. The impactor then bounces back and the load is gradually reduced. Figure 6(a) shows a good agreement obtained between the numerical result and experiment, during the load phase and the estimated maximum force of 3,917N, is slightly lower than that of the test value (4,605N).

Many intense oscillations, highs and drops of force are experimentally observed near the peak, and at approximately 2·2ms the larger force reduction seen can be attributed to the fibre breakage. After the peak load is reached and the impactor starts to rebound the numerical result shows a slightly higher value of load than the experimental and takes a longer time to reach zero. This phenomenon may be due to contact forces between the delaminated plies after the cohesive elements have been removed from the simulation as the composite plate returns to its original shape. Other different impact energy conditions were also performed and the numerical model gave a good correlation with experimental measurements[39].

The impact energy-time relationship under impact energy of 14·7J is presented in Fig. 6(b). The initial kinetic energy of the impactor is transferred to the composite plate once contact is made. During impact, part of this energy is absorbed by the plate in the form of elastic deformation (elastic energy), while a larger amount is dissipated in the form of intra-laminar damage, delamination and the friction between projectile/laminate and among neighbouring plies within the laminate. The kinetic energy of the impactor will finish the completed transfer to the plate when its velocity reaches zero. After this point, the absorbed elastic energy part of the plate is transferred back to the impactor which causes it to rebound. Finally, the energy absorbed by the composite reaches a stable value resulting from the damage and friction. It is clearly shown that a good prediction of the impact energy is obtained from the numerical model when compared to experimental value and the difference between them is less than 5%, suggesting that the assumptions made in the failure

https://doi.org/10.1017/S0001924000007661 Published online by Cambridge University Press

Table 3
Experimental and numerical values of absorbed impact energy[39]

Impact energy (J)	Absorbed energy		Difference between test and simulation (%)
	Experimental (J)	Numerical (J)	
7·35	5·5	4·49	18·36
11·03	7·1	6·02	15·21
14·7	9·52	9·08	4·62

Table 4
Measured and numerically predicted delamination area[39]

Impact energy (J)	Delamination area (mm^2)		
	Experiment	Simulation	
		Complete failure ($d \geq 1$)	Delamination evolution ($0 < d \leq 1$)
7·35	80·36	48	288
11·03	190·46	141	466
14·7	314	251	698

criteria can represent relatively accurately the experimental set up at this impact energy level. The difference between the experimental and numerical energy values becomes bigger at lower applied impact energy levels as can be seen in Table 3[39], suggesting that the extent of damage is underestimated by the model.

4.2 Experimentally detected and numerically predicted damage

Non-destructive evaluation (NDE) of the composite panel by penetrant-enhanced X-ray radiography, shows transverse ply cracking, splitting and almost 'peanut' shaped delaminations, as typically illustrated in Fig. 7(a) when it is impacted under 14·7 J. Figure 7(b) shows the predicted overall damage as comparison, where all the delaminations are represented in rainbow colour (while in print in different shades of grey); dark regions (red) indicate that the material has failed completely while in the lighter grey areas the material comes closer to failure (failure criterion hasn't yet been reached). It is clearly seen that the predicted damage area from the numerical model is well agreed with the measured delamination area by X-ray. The damage area obtained experimentally and numerically for other impact cases was presented in Table 4[39].

Figure 8 shows the permanent indentation captured by the numerical model. The predicted post-impact indentation is similar in depth (1·059mm) to the actual damage observed (approximately 1·1mm) after the impact test. The permanent indentation is formed due to the internal damage and nonlinear shear behaviour of the polymer matrix, where the inelastic shear strain mainly contribute on a permanent indentation and this indentation could play an important role on the performance of the compression after impact event.

https://doi.org/10.1017/S0001924000007661 Published online by Cambridge University Press

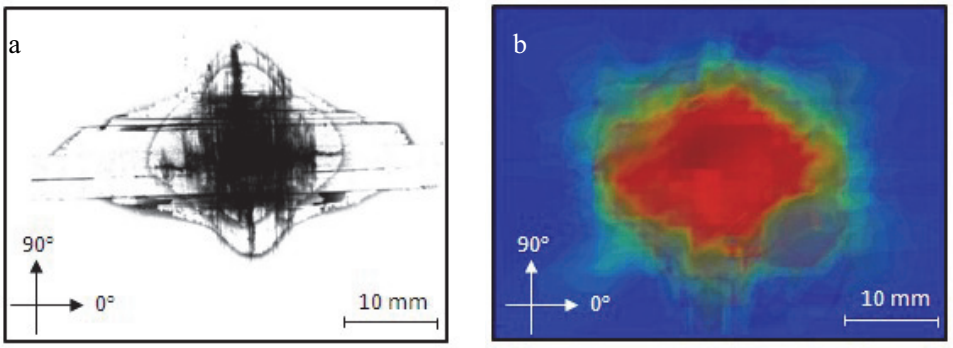

Figure 7. Experimentally measured and numerically captured damage under impact energy of 14·7J (a) X-ray radiograph and (b) numerically predicted image.

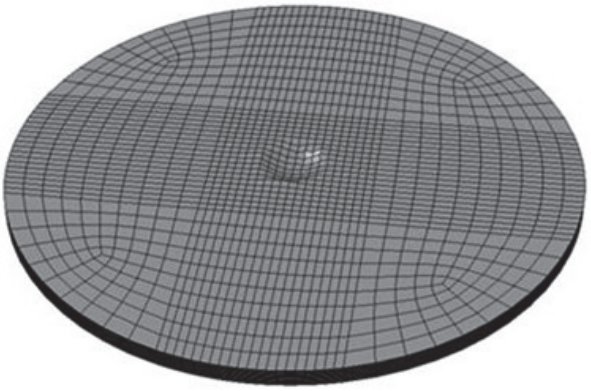

Figure 8. Permanent indentation predicted by numerical model after impact[39].

4.3 Modelling matrix cracks and splitting under impact

As introduced in Section 1.0, in general, the matrix cracking is always recognised as the first resin based damage mode observed in a composite laminate under quasi-static or dynamic loading. Thus it is important to model it in the design of an aircraft structural component, since it may lead to more critical damage, like delamination and fibre breakage.

However, the current intra-laminar damage criteria can only predict the damage area and the overall shape of each damage mode, but not individual cracks and splits that can occur within the ply or at the fibre/matrix interface. Interface cohesive elements have been used to successfully simulate the delamination that develops in the impacted composite laminate as described earlier and in previous work by the authors[39]. In this section, it is shown the intra-laminar damage criteria of Equation (3) in Section 2.1 and the traction-separation law of interface cohesive elements described in Section 2.2 can be used to model transverse matrix cracking and splitting; the cohesive elements are inserted within the ply and between neighbouring finite elements along the fibre direction at predetermined locations (crack spacing) as shown as Fig. 9.

Figure 10 shows the projectile dropped on a 100mm × 100mm square composite plate that is fully clamped by metallic plates, simulating the experimental set-up. The full model is built because the splitting or transverse cracks could unsymmetrically occur and the predicted results can be

https://doi.org/10.1017/S0001924000007661 Published online by Cambridge University Press

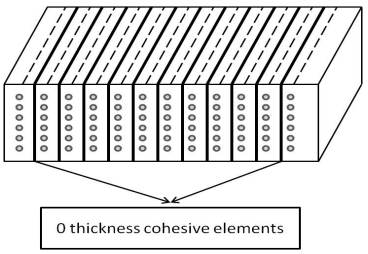

Figure 9. Model matrix cracking or splitting in a single ply with interface cohesive elements.

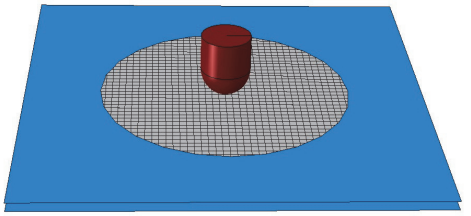

Figure 10. Full impact FE model.

influenced by the clamping conditions. Both clamping plates with a hole of 75mm in diameter are represented by shell elements and fixed to constrain the composite plate. Other specifications and boundary conditions are consistent with the description in Section 3.2.1. Based on the experimental observations, the numerical modelling is meshed with element size of 2mm that allows a maximum crack or splitting density of five cracks/cm. Interface cohesive elements of zero thickness are inserted between adjacent elements along the fibre direction in both 0° and 90° plies, respectively; their elastic modulus and strength are important factors that affect the predicted results and the modulus used is taken equal to 1×10^6 GPa/mm[40]. The strength values related to intra-laminar matrix tensile and out-of-plane shear strength are shown in Table 1, while other fracture properties are presented in Table 2.

Figure 11 shows the experimentally observed and numerically simulated splitting developed at the bottom 0° ply of the $[0/90]_{2s}$ laminate where the maximum out of plane deflection occurs at an impact event of 14·7J. It can be seen from this Fig. 11(b) that the splitting can be successfully modelled, showing a damage pattern similar to that observed in the experiment, Fig. 11(a). The splitting is formed due to large normal tensile and shear stresses, while its propagation is accurately captured by the interface elements embedded within the ply. The fractured material strips created by the splitting measure 76mm in length and 9mm in width, while they are predicted 72mm long and 10mm wide by the numerical model, which can be considered as a good agreement. The analysis in Fig. 11(b), shows regions in the ply where cracks and split started to grow but not yet fully formed and hence not visible in the physical experiment. Thus, the numerical method can be very valuable to help understanding the matrix crack formation and propagation in a composite laminate during a dynamic loading event.

5.0 CONCLUSIONS

In this paper, the impact response and impact induced damage of a carbon fibre/epoxy composite cross-ply $[0/90]_{2s}$ laminate has been experimentally and numerically investigated. A stress based failure criterion was used to predict damage initiation while damage propagation in the form of intra- and inter-laminar cracking is captured by implementing the user subroutine VUMAT of the Abaqus/Explicit commercially available FE code. Delamination is considered as one of the critical failure mechanisms that can substantially reduce the residual strength of the composite plate, especially under compression[41,42], which makes its accurate prediction crucial in the design of composite structures. In the present study, delamination was modelled by inserting cohesive

https://doi.org/10.1017/S0001924000007661 Published online by Cambridge University Press

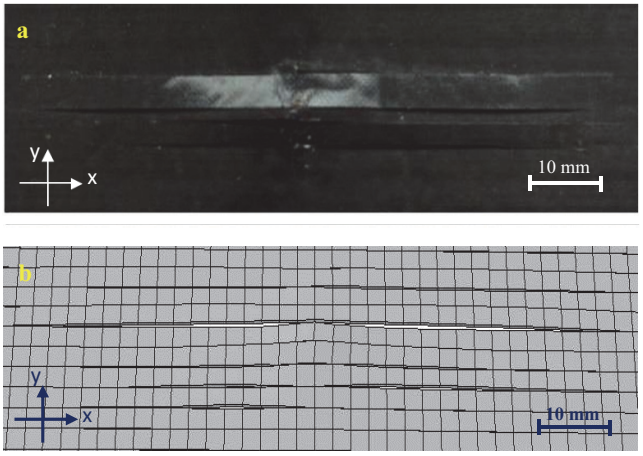

Figure 11. Splitting at the bottom 0° ply when the [0/90]2s laminate is subjected to a 14·7J impact. (a) Experiment and (b) Simulation.

element layers between adjacent plies while transverse matrix cracking or splitting were successfully predicted by inserting the cohesive elements between neighbouring finite elements at predetermined crack spacing inside each single ply. The nonlinear shear response of the composite was also considered by using the Soutis *et al* shear model[4,5] and indentation depth and damage progression compared favourably with the experimental results and observations.

The peak force and energy were all accurately captured in the numerical simulations. The discrepancy between experimental and numerical results is most likely to be due to material properties variability, specimen quality/imperfections introduced during the manufacturing process and/or inaccuracies in the friction coefficient assumed between the projectile and plate or between individual damaged plies. The impact induced damage was also identified by the X-ray radiography technique and its extent and pattern correlated well with the numerical predictions. In addition, the numerical model explicitly simulated the splitting damage mode at the bottom ply of the $[0/90]_{2s}$ laminate when subjected to a 14·7J impact. The assumed stiffness and strength properties of the cohesive elements used estimated reasonably well the splitting extent and pattern. Also the model showed regions in the ply where resin cracks initiated but were not fully developed, something that is more difficult to detect by X-ray radiography or any other non-destructive damage evaluation technique, hence underestimating the severity of internal damage. This may have a significant effect on estimating the residual strength properties and fatigue life of the laminate.

In the near future other multi-directional lay-ups will be attempted, especially thick laminates where a volume effect (scaling effect, especially at ply level) may be an issue[43,44]. Physical tests are also necessary to be performed in order to obtain accurate material parameters for the simulation, like the friction coefficient between projectile and laminate.

In addition, residual strength prediction under uniaxial compressive loading (compression after impact, CAI), often a limiting design parameter in the aircraft construction with composites[45,46], will be studied. The X-ray radiography might be difficult to accurately capture the damage extent and pattern, since the zinc iodide solution used as penetrant may not enter cracks that are partially formed or close after removal of loading. Thus, an effective detection tool such as real time structural health monitoring[1,2] will be necessary for more accurate comparisons of damage size between measurement and numerical simulation. For the numerical technique, a finer

https://doi.org/10.1017/S0001924000007661 Published online by Cambridge University Press

mesh density may be needed to better capture the crack spacing (density). This will require a higher number of cohesive elements and hence higher computational time or more powerful computers. It should be said though that the present study successfully demonstrated that stress and fracture mechanics based criteria with carefully measured/selected material properties and fracture energies can accurately predict the impact response and damage pattern in carbon fibre/epoxy cross-ply laminates.

REFERENCES

1. DIAZ VALDES, S.H and SOUTIS, C. Health monitoring of composites using lamb waves generated by piezo-electric devices, *Plast Rubber Compos*, 2000, **29**, (9), pp 496-502.
2. DIAZ VALDES, S.H and SOUTIS, C. Real-time non-destructive evaluation of fibre composite laminates using low-frequency lamb waves, *J Acc Soc AM*, 2002, **111**, (5), pp 2026-2033.
3. ABRATE, S. *Impact on Composite Structures*, 1998, Cambridge University Press, Cambridge, UK.
4. BERBINAU, P., SOUTIS, C., GOUTAS, P and CURTIS, P.T. Effect of off-axis ply orientation on 0°-fibre microbuckling, *Composites Part A*, 1999, **30**, pp 1197-1207.
5. BERBINAU, P., SOUTIS, C. and GUZ, I.A. Compressive failure of 0° unidirectional carbon-fibre-reinforced plastic (CFRP) laminates by fibre micobuckling, *Compos Sci Technol*, 1999, **59**, pp 1451-1455.
6. ANDERSON T.L. *Fracture Mechanics — Fundamentals and Applications*, 1995, CRC Press, New York.
7. KASHTALYAN, M and SOUTIS, C. The effect of delaminations induced by transverse cracks and splits on stiffness properties of composite laminates, *Composites Part A*, 2000, **31**, pp 107-119.
8. KASHTALYAN, M and SOUTIS, C. Analysis of local delaminations in composite laminates with angle-ply matrix cracks, *Int J Solids Struct*, 2002, **39**, pp 1515-1537.
9. ZHANG, J., FAN, J. AND SOUTIS, C. Analysis of multiple matrix cracking in $[\pm\theta_m/90_n]_s$ composite laminates. Part 1: In-plane stiffness properties, *Composites*, 1992, **23** ,(5), pp 291–298.
10. KASHTALLYAN, M.Y. and SOUTIS, C. Mechanisms of internal damage and their effect on the behaviour and properties of cross-ply composite laminates, *Int Appl Mech*, 2002, **38**, (6), pp 641-657.
11. ZHANG, J., SOUTIS, C. and FAN, J. Strain energy release rate associated with local delamination in cracked composite laminates, *Composites*, 1994, **25**, (9), pp 851-862.
12. TITA, V., DE CARVALHO, J. and VANDEPITTE, D. Failure analysis of low velocity impact on thin composite laminates: Experimental and numerical approaches, *Compos Struct*, 2008, **83**, pp 413-428.
13. DAVIES, G.A.O. and OLSSON, R. Impact on composite structures, *Aeronaut J*, 2004, **108**, (1089), pp 541–563.
14. MATTHEWS, F.L., DAVIES, G.A.O., HITCHINGS, D. and SOUTIS, C. *Finite Element Modelling of Composite Materials and Structures*, 2000, Woodhead Publishing, Cambridge.
15. DONADON, M.V., IANNUCCI, L., FALZON, B.G., HODGKINSON, J.M. and ALMEIDA, S.F.M. A progressive failure model for composite laminates subjected to low velocity impact damage, *Comput Struct*, 2008, **86**, pp 1232-1252.
16. FAGGIANI, A. and FALZON, B.G. Predicting low-velocity impact damage on a stiffened composite panel, *Composites Part A*, 2010, **41**, pp 737-749.
17. IANNUCCI, L. and ANKERSEN, J. An energy based damage model for thin laminated composites, *Compos Sci Technol*, 2006, **66**, pp 934-951.
18. YOKOYAMA, N.O., DONADON, M.V. and ALMEIDA, S.F.M. A numerical study on the impact resistance of composite shells using an energy based failure model, *Compos Struct*, 2010, **93**, pp 142-152.
19. KACHANOV, L.M. On the creep rupture time, *Izv AN SSSR Otd Tekhn Nauk*, 1958, **8**, pp 26-31.
20. RABOTNOV, Y.N. On the equations of state for creep, *Progress in Applied Mechanics*, 1963, Prager Anniversary Volume, Macmillan, NewYork.
21. KASHTALYAN, M. and SOUTIS, C. Analysis of composite laminates with intra- and interlaminar damage, *Prog Aerosp Sci*, 2005, **41**, pp 152-173.
22. HASHIN, Z. and ROTEM, A. A fatigue failure criterion for fiber-reinforced materials, *J Compos Mater*, 1973, **7**, pp 448-464.
23. HASHIN, Z. Failure criteria for uni-directional fibre composites, *J Appl. Mech*, 1980, **47**, (1), pp 329–334.
24. PUCK, A. and SCHURMANN, H. Failure analysis of FRP laminates by means of physically based phenomenological models, *Compos Sci Technol*, 1998, **58**, (10), pp 1045–1067.

25. BAŽANT, Z.P. and OH, B.H. Crack band theory for fracture of concrete, *Mater Struct*, 1983, **16**, pp 155–177.
26. LAPCZYK, I. and HURTADO, J.A. Progressive damage modelling in fiber-reinforced materials, *Composites Part A*, 2007, **38**, pp 2333-2341.
27. CAMANHO, P.P. and DÁVILA, C.G. Mixed-Mode decohesion finite elements for the simulation of delamination in composite materials, 2002, Tech Report NASA/TM-2002-211737.
28. ABAQUS. ABAQUS Version 6.10, 2010, Dessault systems, Providence, RI, USA.
29. KHAN, S.A. and HUANG, S. *Continuum Theory of Plasticity*, 1995, John Wiley and Sons, New York, USA.
30. LEMAITRE, J. and CHABOCHE, J.L. *Mechanics of Solid Materials*, 1990, Cambridge University Press, Cambridge, UK.
31. DANESI, R., LUCCIONI, B. and OLLER, S. Coupled plastic-damaged model, *Comput Methods Appl Mech Eng*, 1996, **129**, (1-2), pp 81-89.
32. ASTM D7136/D7136M-07. Standard test method for measuring the damage resistance of a fibre-reinforced polymer matrix composite to a drop-weight impact event, 2007, American Society for Testing and Materials, Philadelphia, USA.
33. JUMAHAT, A., SOUTIS, C. and HODZIC, A. A graphical method predicting the compressive strength of toughened unidirectional composite laminates, *Appl Compos Mater*, 2011, **18**, pp 65-83.
34. CHANG, F.K. and SHAHID, I.S. An accumulative damage model for tensile and shear failures of laminated composite plates, *J Compos Mater*, 1995, **29**, (7), pp 926–981.
35. PINHO, S.T., IANNUCCI, L. and ROBINSON, P. Fracture toughness of the tensile and compressive fibre failure modes in laminated composites, *Compos Sci Technol*, 2006, **66**, (13), pp 2069–2079.
36. SUNG, N. and SUH, N. Effect of fiber orientation on friction and wear of fiber reinforced polymeric composites, *Wear*, 1979, **53**, pp 129–141.
37. SCHON, J. Coefficient of friction of composite delamination surfaces, *Wear*, 2000, **237**, pp 77–89.
38. BING, Q. and SUN, C.T. Effect of transverse normal stress on mode II fracture toughness in fiber composites, 2007, 16th International conference on composite materials, Kyoto, Japan.
39. SHI, Y., SWATI, T. and SOUTIS, C. Modelling damage evolution in composite laminates subjected to low velocity impact, *Compos Struct*, 2012, **94**, pp 2902-2913.
40. CAMANHO, P.P., DÁVILA, C.G. and DE MOURA, M.F. Numerical simulation of mixed-mode progressive delamination in composite materials, *J Compos Mater*, 2003, **37**, (16), pp 1415-1438.
41. SOUTIS, C. and GUZ, I.A. Fracture of layered composites by internal fibre instability: Effect of interlaminar adhesion, *Aeronaut J*, 2006, **110**, (1105), pp 185-195.
42. SOUTIS, C., SMITH, F.C. and MATTHEWS, F.L. Predicting the compressive engineering performance of carbon fibre-reinforced plastics, *Composites Part A*, 2000, **31**, (6), pp 531-536.
43. LAVOIE, J.A., SOUTIS, C. and MORTON, J. Apparent strength scaling in continuous fiber composite laminates, *Compos Sci Technol* ,2000, **60**, (2), pp 283-299.
44. LEE, J. and SOUTIS, C. A study on the compressive strength of thick carbon fibre/epoxy laminates. *Compos Sci Technol*, 2007, **67**, (10), pp 2015-2026.
45. CURTIS, P.T., HAWYES, V.J. and SOUTIS, C. Effect of impact damage on the compressive response of composite laminates. *Composites Part A*, 2001, **32**, (9): 1263-1270.
46. SOUTIS, C. and CURTIS, P.T. Prediction of the post-impact compressive strength of CFRP laminated composites, *Compos Sci Technol*, 1996, **56**, (6), pp 677-684.